Can Cyclen Bind Alkali Metal Azides?

A DFT Study as a Precursor to Synthesis

H. Bhakhoa,[a] L. Rhyman,[a] E. P. F. Lee,[b,c] P. Ramasami[a,d*] and J. M. Dyke[b*]

[a]Computational Chemistry Group, Department of Chemistry, Faculty of Science, University of Mauritius, Réduit 80837, Mauritius
[b]School of Chemistry, University of Southampton, Highfield, Southampton SO17 1BJ, UK
[c]Department of Applied Biology and Chemical Technology, The Hong Kong Polytechnic University, Hung Hom, Kowloon, Hong Kong
[d]Visiting Professor, Department of Pharmaceutical Chemistry, College of Pharmacy, King Saud University, P.O. Box 2457, Riyadh 11451, Saudi Arabia

Corresponding Author(s)
*E-mail: ramchemi@intnet.mu (P.R.); jmdyke@soton.ac.uk (J.M.D.)

Graphical Abstract

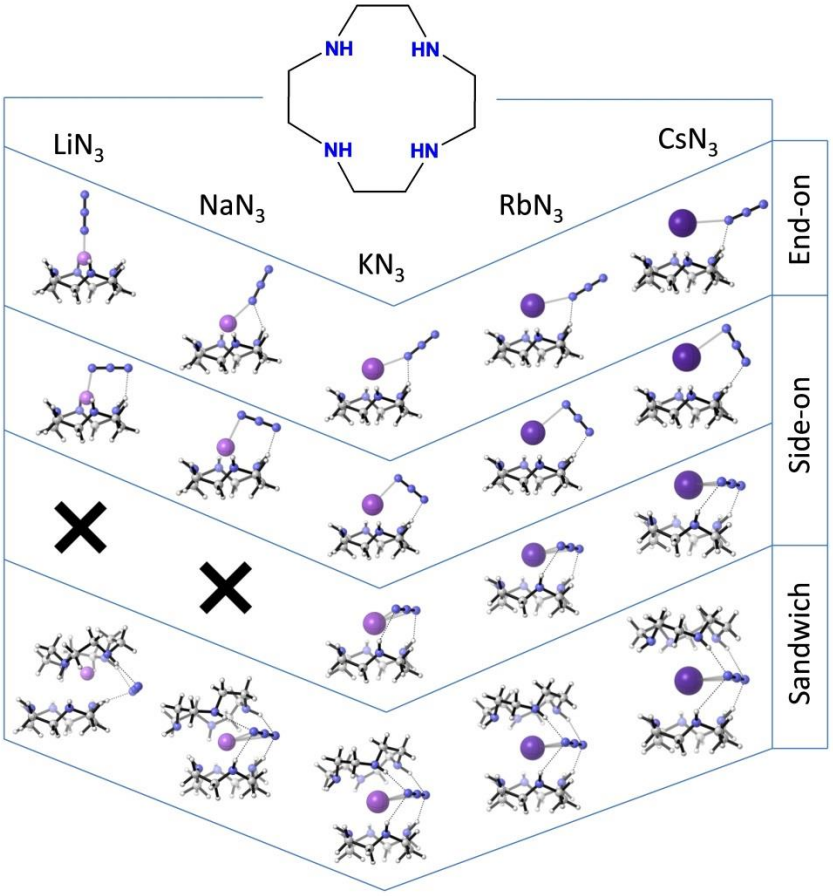

Abstract

Can cyclen (1,4,7,10-tetraazacyclododecane) bind alkali metal azides? This question is addressed by studying the geometric and electronic structures of the alkali metal azide-cyclen [M(cyclen)N_3] complexes using density functional theory (DFT). The effects of adding a second cyclen ring to form the sandwich alkali metal azide-cyclen [M(cyclen)$_2N_3$] complexes are also investigated. N_3^- is found to bind to a M^+(cyclen) template to give both end-on and side-on structures. In the end-on structures, the terminal nitrogen atom of the azide group (N1) bonds to the metal as well as to a hydrogen atom of the cyclen ring *via* a hydrogen bond in an end-on configuration to the cyclen ring. In the side-on structures, the N_3 unit is bonded, in a side-on configuration to the cyclen ring, to the metal *via* the terminal nitrogen atom of the azide group (N1), and *via* the other terminal nitrogen atom (N3) of the azide group by a hydrogen bond to a hydrogen atom of the cyclen ring. For all the alkali metals, the N_3-side-on structure is lowest in energy. Addition of a second cyclen unit to [M(cyclen)N_3] to form the sandwich compounds [M(cyclen)$_2N_3$] causes the bond strength between the metal and the N_3 unit to decrease. It is hoped that this computational study will be a precursor to the synthesis and experimental study of these novel macrocyclic compounds. Structural parameters and infrared spectra are computed for these complexes which will assist the experimental work.

Keywords

Host-guest chemistry, azamacrocycle, alkali metal azide, DFT calculations, cyclen complexes

1.0 Introduction

The design of macrocycles with the ability for selective complexation is of utmost importance in the realm of host-guest chemistry. Crown ethers, cyclic oligomers of dioxane in its simplest form,[1] remain one of the most widely studied macrocycles and are well-known for their ability to complex the 'hard' alkali metal ions in a specific and selective manner. The ubiquitous nature of the alkali metal-crown ether combination has opened the door to innumerable applications.[2] Metal complexes of macrocycles, such as crown ether, have the ability to activate anions by increasing their nucleophilicity.[3] However, few studies[4] have efficiently explored macrocycles as activating agents to trigger the formation of potentially high energy density polynitrogen compounds[5] such as N_6 from alkali metal azide precursors. The synthesis and characterisation of the metal azide-crown ether complexes of Li(12crown4), Na(15crown5) and M(18crown6), where M = K, Rb and Cs, was perhaps the first effort in this direction.[4a] The crystal structures obtained were compared with structures obtained by density functional theory (DFT) calculations. These calculations also probed the electronic structure of these complexes and demonstrated the versatility of the azide ligand which can coordinate to the alkali metal-crown ether complexes either in an end-on or a side-on mode.

Cyclen is the tetra-aza analogue of 12crown4 ether. As substitution of oxygen, in a macrocyclic ligand such as crown ether, for nitrogen is known to impart extra stability to the corresponding alkali metal complexes,[6] the question arises: Can unfunctionalised N-donor macrocycles form stable complexes with alkali metal derivatives? In light of this, we investigated the alkali metal azide complexes of cyclen (1,4,7,10-tetraazacyclododecane), a representative of azamacrocycles. A renaissance of interest in metal complexes of cyclen and its derivatives has been fueled mainly by their importance in medicine where they are used, for example, as MRI contrast agents, and anti-HIV and anticancer drugs.[7] The ligational behaviour of functionalised cyclen towards alkali metal cations has been investigated previously by electronic and NMR spectroscopy, potentiometric titrations, X-ray crystallography and theoretical methods.[8] In contrast, studies related to the interaction between the parent cyclen and alkali metal cations are scarce in literature,[9] except for two recent investigations conducted by Austin and coworkers.[10] These were studies of threshold collision-induced dissociation with xenon and infrared multiphoton dissociation spectroscopy respectively of the alkali metal ion-cyclen complexes, M^+(cyclen), for $M^+ = Na^+$, K^+, Rb^+ and Cs^+. The results obtained were

interpreted using DFT calculations. For all M^+(cyclen) complexes studied, the lowest minimum energy structure was found to be a C_4(++++) structure where all four N-donor atoms of the cyclen are oriented toward the alkali metal atom. The (++++) indicates that all four amino hydrogen atoms are located above the plane of the cyclen ring.

While no studies have previously been reported on alkali metal azide-cyclen complexes, several transition metal azide-NNNN macrocyclic analogues are known. In these investigations, it was found that the azide ligand takes up an axial position on the transition metal macrocycle through strong interaction between the transition metal and the terminal N of the azide.[11] Some of these complexes have been used in simple experiments which mimic reactions of naturally occurring metalloenzymes, where the azide group was mainly employed in ligand exchange reactions at the active sites.[11c,g,j] The dissociative pathways of the photolabile azide ligand have also been highlighted in several reports.[11a-c,g-i] It was even proposed that the photodissociation products of the azide moiety could potentially lead to the formation of polynitrogen species.[11i] Some alkali metal ion-azamacrocyclic complexes such as $M^+(Me_3tacn)_2$[6,12] and $Cs^+(HMHCY)_2$[13] have been reported (Me_3tacn = 1,4,7-trimethyl-1,4,7-triazacyclononane and HMHCY = 1,4,7,10,13,16-hexamethyl-1,4,7,10,13,16-hexaazacyclooctadecane). Despite the fact that it is well-known that the alkali metal cations can form homo-sandwich complexes of the type $M^+(12crown4)_2$,[14] no studies pertaining to sandwich structures of alkali metal derivatives of NNNN-containing macrocycles have appeared in literature. So far, it is only for complexes of rare earth metals with homo and hetero-sandwich complexes with NNNN-containing macrocycles such as porphyrins and phthalocyanines that the synthesis and geometric structures have been reported, electronic properties investigated and spectroscopic studies carried out.[15]

In this work, we report DFT computed structures of N_3-end-on and N_3-side-on alkali metal azide-cyclen [M(cyclen)N_3] complexes, where M = Li, Na, K, Rb and Cs. Density fitted and locally correlated CCSD(T) [DF-L(U)CCSD(T)] calculations were also employed to obtain accurate bond dissociation energies (BDEs) for N_3 loss from these structures. The effects of adding an additional cyclen macrocycle to yield the sandwich alkali metal azide-cyclen [M(cyclen)$_2N_3$] complexes were also investigated. We hope that this study will be a precursor to the future synthesis of these complexes, as valuable information is provided on the structure and bonding in these macrocyclic complexes.

2.0 Computational Detail

The DFT generalised gradient functional BP86[16] of Becke and Perdew was used to perform Berny geometry optimisations[17] for all the chemical species investigated in this work. The standard triple-ζ plus polarisation Pople-style 6-311G(d,p) basis set[18] was employed for H, C, N, Li, Na and K atoms, while Cs and Rb atoms were treated by using Stuttgart Relativistic Small Core (RSC) 1997 Effective Core Potentials (ECPs). The ECPs not only model the core electrons and treat the valence electrons in an explicit manner, but they also take into consideration scalar relativistic effects which are important in high atomic number elements.[19] The reliability of the BP86 functional[11f] with the 6-311G(d,p) and the Stuttgart RSC 1997 ECP basis sets in molecules of the type studied in this work has been established in recent studies involving metal azide-macrocyclic complexes.[4a,c] The DFT calculations were repeated using the Becke three parameter non-local hybrid exchange correlation functional, B3LYP.[20] In particular, the geometries of the M^+(cyclen) complexes, for M^+ = Li^+-Cs^+, were additionally optimised using the B3LYP/DEF2-TZVPPD method, given that minimum energy structures of M^+(cyclen) for M^+ = Na^+, K^+, Rb^+ and Cs^+ have been previously computed using this functional and basis set by Austin *et al.*[10a] The DEF2-TZVPPD[21] is a triple-ζ basis set which includes polarisation and diffuse functions and uses ECPs on Rb and Cs as developed by Leininger and coworkers.[19] For all these DFT calculations, geometry optimisation was followed by analytic Hessian computation for each complex, and the absence of negative Hessian eigenvalues confirmed the stationary points as minima on the corresponding potential energy hypersurfaces. Bond dissociation energies (BDEs) were calculated for the following processes using the BP86/6-311G(d,p) and B3LYP/6-311G(d,p) methods:

$$[M(cyclen)(N_3)]_{(g)} \rightarrow M(cyclen)_{(g)} + N_{3(g)} \quad (1)$$

$$[M(cyclen)(N_3)]_{(g)} \rightarrow M(cyclen)N_{(g)} + N_{2(g)} \quad (2)$$

$$[M(cyclen)_2(N_3)]_{(g)} \rightarrow M(cyclen)_{2(g)} + N_{3(g)} \quad (3), \quad \text{where M = Li-Cs.}$$

Natural bond analysis (NBO) was also carried out following the method of Weinhold and coworkers.[22] Zero-point energy (ZPE) corrections are included in all reported energies and are given at 298.15 K and 1 atm. All the above-mentioned computations were performed using the Gaussian 09 package.[23]

Single-point DF-L(U)CCSD(T) (density fitted and locally correlated coupled cluster with single, double and perturbative non-iterative local triple excitations)[24] calculations were performed at the BP86/6-311G(d,p) optimised geometries using the MOLPRO 2012.1 program.[25] The "DF" approximation is known to reduce the computational costs pertaining to the computation and processing of electron interaction integrals (ERIs) and has been widely used in combination with local correlated methods.[26] The "local" approximation reduces the computational cost with molecular size.[27] The DZ and TZ basis sets employed in the DF-L(U)CCSD(T) calculations are summarised in the Supplementary Information (SI). For Li and Na, all electron cc-pwCVXZ basis sets, with X = D or T, were used. For K, Rb and Cs, flexible metal core-valence basis sets, for use with effective core potentials ECPnMDF, were designed to be suitable for both M^+ and M (see SI for details). They are denoted ACVXZ (with X = D or T). It should be noted that by default, for M, the valence ns^1 electron is the only electron to be correlated, while for M^+, the $(n-1)s^2$ and $(n-1)p^6$ electrons become valence electrons. In order for electron correlation to be accounted for in a consistent and balanced manner for both M and M^+, the $(n-1)s^2(n-1)p^6$ and ns^1 electrons were correlated for both M and M^+ in all DF-L(U)CCSD(T) calculations employing core-valence basis sets for M/M^+. The DF-L(U)CCSD(T) method was used to obtain accurate BDEs for the process (1) above, as a check on the DFT values for this dissociation. Relative electronic energies [$\Delta E^{corr}(n)$] obtained with the ACVDZ and ACVTZ basis sets were extrapolated to the complete basis set (CBS) limit employing the two-parametric expression:[28]

$$\Delta E^{corr}(n) = \Delta E^{corr}_{CBS} + An^{-3} \qquad (4)$$

where *n* corresponds to the cardinality of the basis set used; for instance *n* = 2 for ACVDZ. In this way, dissociation energies were obtained for process (1) at the CBS level.

All computations were carried out by means of the resources provided (Gaussian 09 and MOLPRO 2012.1 programs) by GridChem Science Gateway[29] and the UK National Service for Computational Chemistry Software† (NSCCS).

3.0 Results and Discussion

This section is organised as follows: Section 3.1 presents the relative energies and structural parameters of (a) the lowest Li^+(cyclen) minimum energy structures, (b) the lowest N_3-

end-on [M(cyclen)N_3] minimum energy structures, (c) the lowest N_3-side-on [M(cyclen)N_3] minimum energy structures, (d) the N_3-side-on versus the N_3-end-on structures and (e) the sandwich [M(cyclen)$_2N_3$] structures (M = Li-Cs). Then, sections 3.2 and 3.3 focus on the bonding analysis and infrared (IR) spectra of the [M(cyclen)N_3] and [M(cyclen)$_2N_3$] structures, respectively. A discussion on the BDEs of these structures is provided in the last section, section 3.4.

3.1 Structures and Energetics

(a) Li^+(cyclen) structures

Geometry optimisation calculations were carried out on the Li^+(cyclen) complex to compare with the work of Austin and coworkers.[10] The lowest energy Li^+(cyclen) structures (**Li-a** to **Li-d**) obtained using the BP86/6-311G(d,p) method are displayed in Figure 1. In general, the B3LYP functional with both the 6-311G(d,p) and DEF2-TZVPPD basis sets gives similar minimum energy geometries, the same energy order for these structures and relative energies which are very close to the BP86 relative energies. As in the previous calculations[10a] on these complexes for M^+ = Na^+-Cs^+, the C_4(++++) structure (**Li-a**) is computed to be the lowest energy structure with the C_{2v}(++++) structure (**Li-b**) being the next highest energy minimum, at 11.3 kJ.mol^{-1} (BP86 value; B3LYP value, 11.4 kJ.mol^{-1}) above the C_4(++++) form. Geometry optimisation calculations were repeated on the M^+(cyclen) minimum energy structures reported by Austin *et al.*[10a] (M^+ = Na^+-Cs^+) using the BP86/6-311G(d,p), B3LYP/6-311G(d,p) and B3LYP/DEF2-TZVPPD methods. The corresponding structures and relative energies are provided in SI (Figures S1-S4). The results obtained using the three methods are comparable. Austin *et al.*[10a] results are also reproduced satisfactorily in this work.

The four Li^+(cyclen) minimum energy structures are very similar to those of the M^+ = Na^+-Cs^+ complexes, although the same energy order for these structures is not observed. The C_4(++++) structure is the lowest energy structure for each alkali metal for the three types of DFT calculations performed. For Li^+(cyclen) (Figure 1), the C_{2v}(+-+-) structure (**Li-d**) is more stable than the C_s(+++-) structure (**Li-c**), while for the M = Na-Cs complexes, the opposite is observed with the C_s(+++-) structure (**M-c**) being more stable than the corresponding C_{2v}(+-+-) structure (**M-d**). The Li^+ ion, having a small ionic radius of 0.60 Å,[9a] fits completely within the plane formed by the four N-donor atoms of the cyclen ring for the C_{2v}(+-+-) structure (**Li-d**). In

contrast, for the C_{2v}(+-+-) structures (**M-d**), the M^+ ion lies well above the donor plane with distances of 1.224 (**Na-d**), 1.843 (**K-d**), 2.459 (**Rb-d**) and 2.792 Å (**Cs-d**), respectively (BP86; B3LYP/6-311G(d,p), 1.506, 2.083, 2.506 and 2.870 Å, respectively).

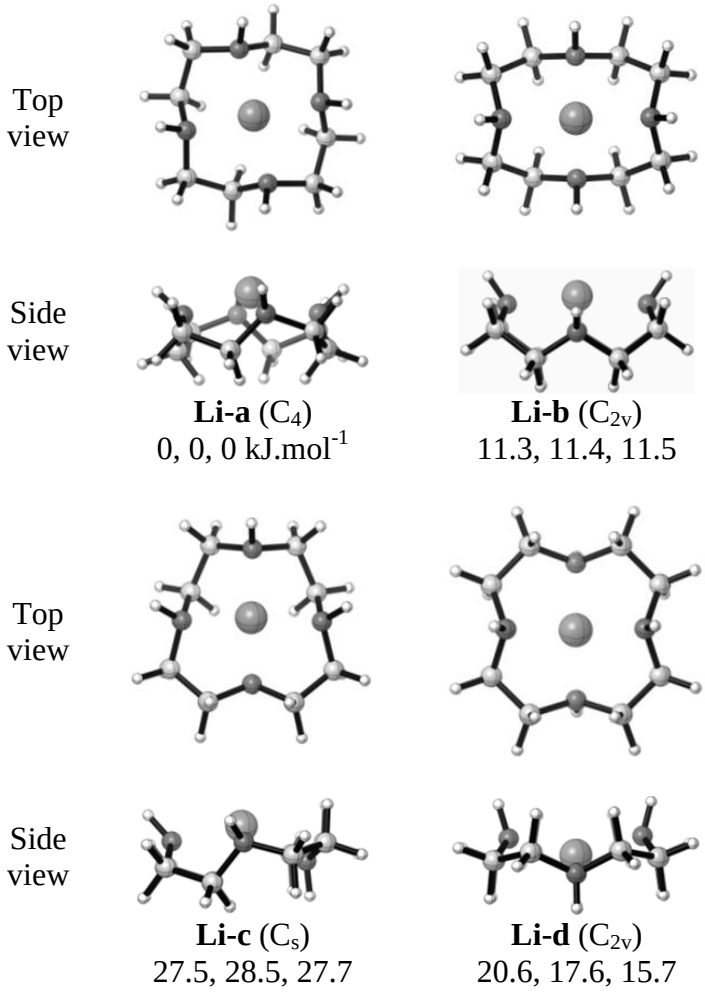

Figure 1 Optimised geometries [BP86/6-311G(d,p)] and relative energies (kJ.mol^{-1}) of the Li^+(cyclen) minimum energy structures. The B3LYP relative energies in conjunction with 6-311G(d,p) (second number) and DEF2-TZVPPD (third number) basis sets are also provided. The symmetry of each structure is given in brackets.

The M^+(cyclen) minimum energy structures (M^+ = Li^+-Cs^+) were used as starting points to generate several N_3-end-on and N_3-side-on [M(cyclen)N_3] structures using the BP86/6-311G(d,p) and B3LYP/6-311G(d,p) methods. As the size of the alkali metal cation increases, the number of N_3-end-on and N_3-side-on minimum energy structures increases. For instance, six N_3-

end-on and eight N_3-side-on [Li(cyclen)N_3] minimum energy structures were obtained, while for [Cs(cyclen)N_3], there are twelve N_3-end-on and seventeen N_3-side-on minimum energy structures. The lowest minimum energy N_3-end-on and N_3-side-on structures will be discussed in this work. In general, good agreement was obtained between the two functionals in terms of bond angles and bond distances for each minimum energy structure (Tables S1-S4). The low-lying [M(cyclen)N_3] structures are provided in SI.

(b) N_3-end-on [M(cyclen)N_3] structures, M = Li-Cs

The geometry and selected structural parameters of the lowest minimum energy N_3-end-on structures are displayed in Figures 2 and 3, with the relative energies of all minimum energy N_3-end-on structures being given in SI (Figures S5, S7, S9, S11 and S13). For M = Li, the lowest energy structure is **Li-1a** with another structure **Li-1b** lying slightly higher in energy. The **Li-1a** structure (Figure 2a) possesses C_4 symmetry with the Li^+ ion lying 0.954 Å (BP86; B3LYP, 0.948 Å) above the plane defined by the four N-donor atoms of the cyclen ring, similar to the C_4(++++) Li^+(cyclen) structure (**Li-a**). The Li^+ ion in the C_4(++++) structure (**Li-a**) of Li^+(cyclen) lies 0.639 Å above the basal plane as compared to 0.954 Å in **Li-1a** of [Li(cyclen)N_3]. The Li^+ centre in **Li-1a** is further coordinated to the terminal N1 atom of the N_3 group with a Li-N1-N2 bond angle of 180° and Li-N1 bond distance of 1.864 Å (BP86; B3LYP, 1.852 Å). The next stable N_3-end-on structure **Li-1b** (Figure 2b) is computed to be only 1.1 kJ.mol^{-1} higher in energy than **Li-1a**, with the BP86 functional. Optimisation of **Li-1b** with the B3LYP functional gave a structure similar to **Li-1a**, indicating that the [M(cyclen)N_3] structures obtained are dependent on the functional used. The main structural difference between **Li-1a** and **Li-1b** lies in the geometrical arrangement of the N_3 group with the latter having a Li-N1-N2 bond angle of 159.6° (Figure 2). Structure **Li-1a** is compared with the structure of its 12crown4 (12C4) analogue, [Li(12C4)N_3], in Figure 2.[4a]

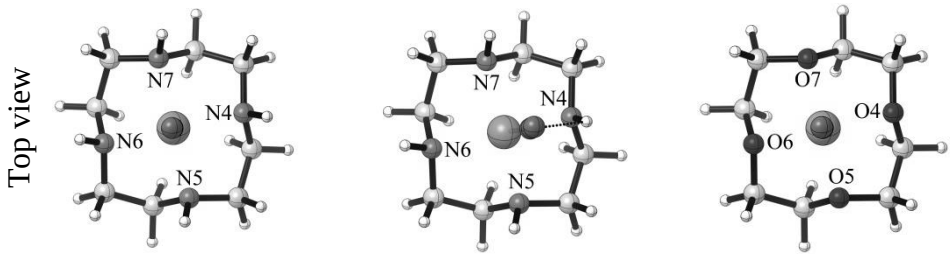

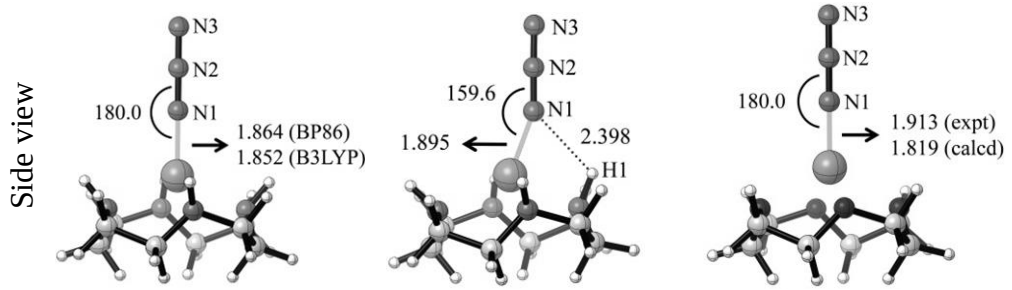

a) Li-1a (C_4) **b) Li-1b** (C_1) **c) [Li(12C4)N_3]** (C_4)

Figure 2 (a) and (b) Optimised geometries [BP86/6-311G(d,p)] of the two minimum energy N_3-end-on [Li(cyclen)N_3] structures. (c) Optimised geometry [BP86/6-311G(d,p)] of the [Li(12C4)N_3] complex, reported in reference 4a. Bond angles are in degree (°) and bond distances are in angstrom (Å). The symmetry is given in brackets.

The geometries of the lowest minimum energy N_3-end-on structures **Na-1a**, **K-1a**, **Rb-1a** and **Cs-1a** (Figure 3) are different from that of their **Li-1a** analogue in terms of the geometrical arrangement of the N_3 group. The structures **M-1a**, for M = Na-Cs, show greater similarity with structure **Li-1b** than **Li-1a**. As the ionic radii of the alkali metal cations increase, the lowest minimum energy N_3-end-on structure changes from a structure with the N_3 group perpendicular to the plane of the four N-donor atoms in the cyclen ring, towards structures with the N_3 unit angled away from the vertical because of the interaction of the terminal N1 atom of the N_3 group with the H1 atom of the N4-H1 group in the cyclen ring. A balance is achieved between the displacement of the M^+ = Li^+-Cs^+ ions out of the basal plane and the H1···N1 interaction such that the M-N1-N2 bond angles (BP86, B3LYP, *ca.* 160°) remain approximately constant throughout the series. The H1···N1 distances in the N_3-end-on structures change from 2.398 → 2.062 (2.231) → 1.937 (2.031) → 1.905 (1.992) → 1.897 (1.974) Å on going from **Li-1b** → **Na-1a** → **K-1a** → **Rb-1a** → **Cs-1a** (BP86 values, with B3LYP values in brackets). This steady decrease in N1···H1 distances on going from Li^+ → Cs^+ is accompanied by an increase in the displacement of the M^+ ion out of basal plane of the cyclen ring (Table 1). Additionally, the N1-N2 and N2-N3 distances of the structures **M-1a**, for M = Na-Cs, are comparable to those of **Li-1a** and **Li-1b** (Tables S1-S2).

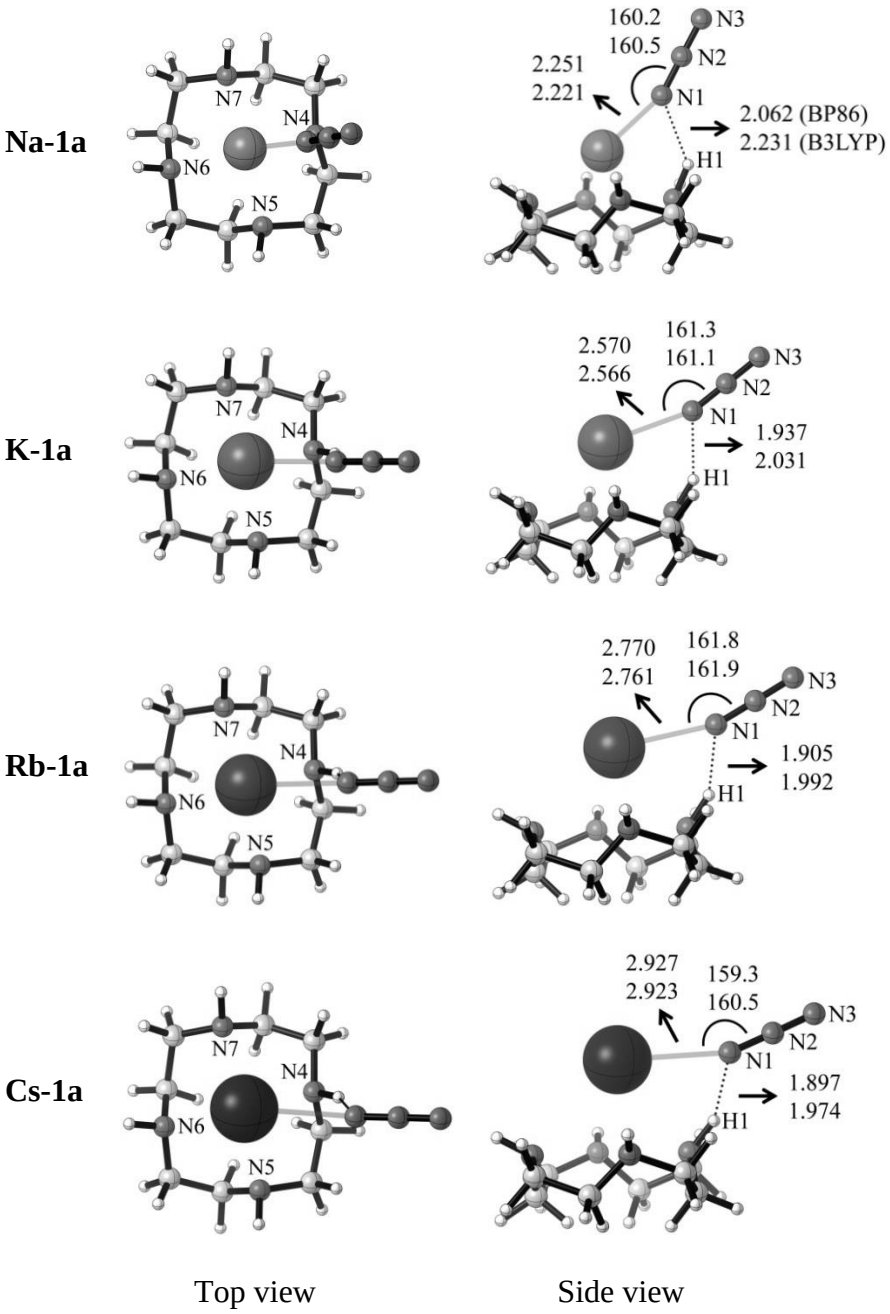

Figure 3 Optimised geometries [BP86/6-311G(d,p)] of the lowest minimum energy N_3-end-on structures. Selected bond angles (°) and bond distances (Å) are provided for both BP86 and B3LYP functionals.

Table 1 The distance (Å) between the plane of the four N-donor atoms of the cyclen ring and the M^+ ions of the lowest minimum energy N_3-end-on structures.

N_3-end-on structures	**Li-1a**	**Li-1b**[a]	**Na-1a**	**K-1a**	**Rb-1a**	**Cs-1a**	$[Li(12C4)N_3]$[b]

BP86/6-311G(d,p)	0.954	0.938	1.370	1.916	2.178	2.434	0.858(4)
B3LYP/6-311G(d,p)	0.948	–	1.352	1.932	2.196	2.460	

[a] The distance (Å) corresponds to the next highest energy N_3-end-on [Li(cyclen)N_3] structure, **Li-1b** with respect to **Li-1a**.
[b] The distance (Å) corresponds to the crystal structure of [Li(12C4)N_3], reported in reference 4a.

(c) N_3-side-on [M(cyclen)N_3] structures, M = Li-Cs

The geometry and selected structural parameters of the lowest minimum energy N_3-side-on structures are displayed in Figures 4 and 5. The N_3-side-on structures **Li-2a** and **Na-2a** are isostructural and hence, will be discussed together. Their M^+(cyclen) units show close similarity to the C_4(++++) M^+(cyclen) structures (**Li-a/Na-a**). The ability of the N_3 unit to act as a μ-1,3-bridging ligand (end-to-end coordination mode), between the penta-coordinated Li^+/Na^+ centre and the H1 atom of the cyclen ring, is clearly observed in **Li-2a** and **Na-2a**. The H1···N3 interaction in **Li-2a** and **Na-2a** (Figure 4) is characteristic of hydrogen bonding and these computed distances are consistent with several reported (N-H)···N distances (2.13, 2.11 and 2.05 Å) in other compounds.[30]

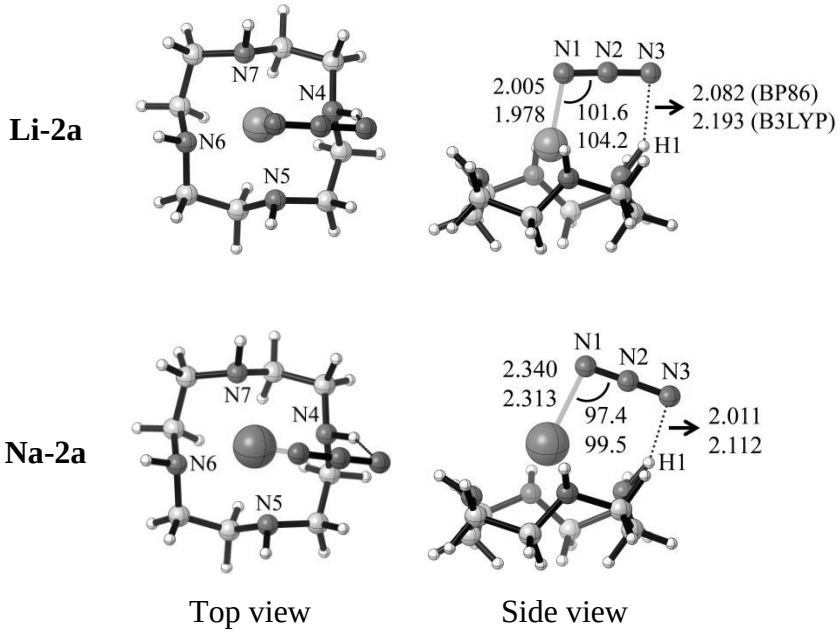

Figure 4 Optimised geometries [BP86/6-311G(d,p)] of the lowest minimum energy N_3-side-on structures (M = Li, Na). Selected bond angles (°) and bond distances (Å) are provided.

As shown in Figure 5, the lowest minimum energy N_3-side-on structures **K-2a**, **Rb-2a** and **Cs-2a** are nearly isoenergetic with their next highest energy structures **K-2b**, **Rb-2b** and **Cs-2b** with small energy gaps of 1.3 (1.5), 1.0 (0.5) and 1.1 (1.2) kJ.mol^{-1}, respectively (BP86 values, with B3LYP values in brackets). In contrast, the N_3-side-on structures **Li-2a** and **Na-2a** are calculated to be 9.8 (9.9) and 18.4 (18.9) kJ.mol^{-1} (BP86 values, with B3LYP values in brackets) lower in energy than their corresponding next highest energy structures **Li-2b** and **Na-2b** (Figures S7 and S9).

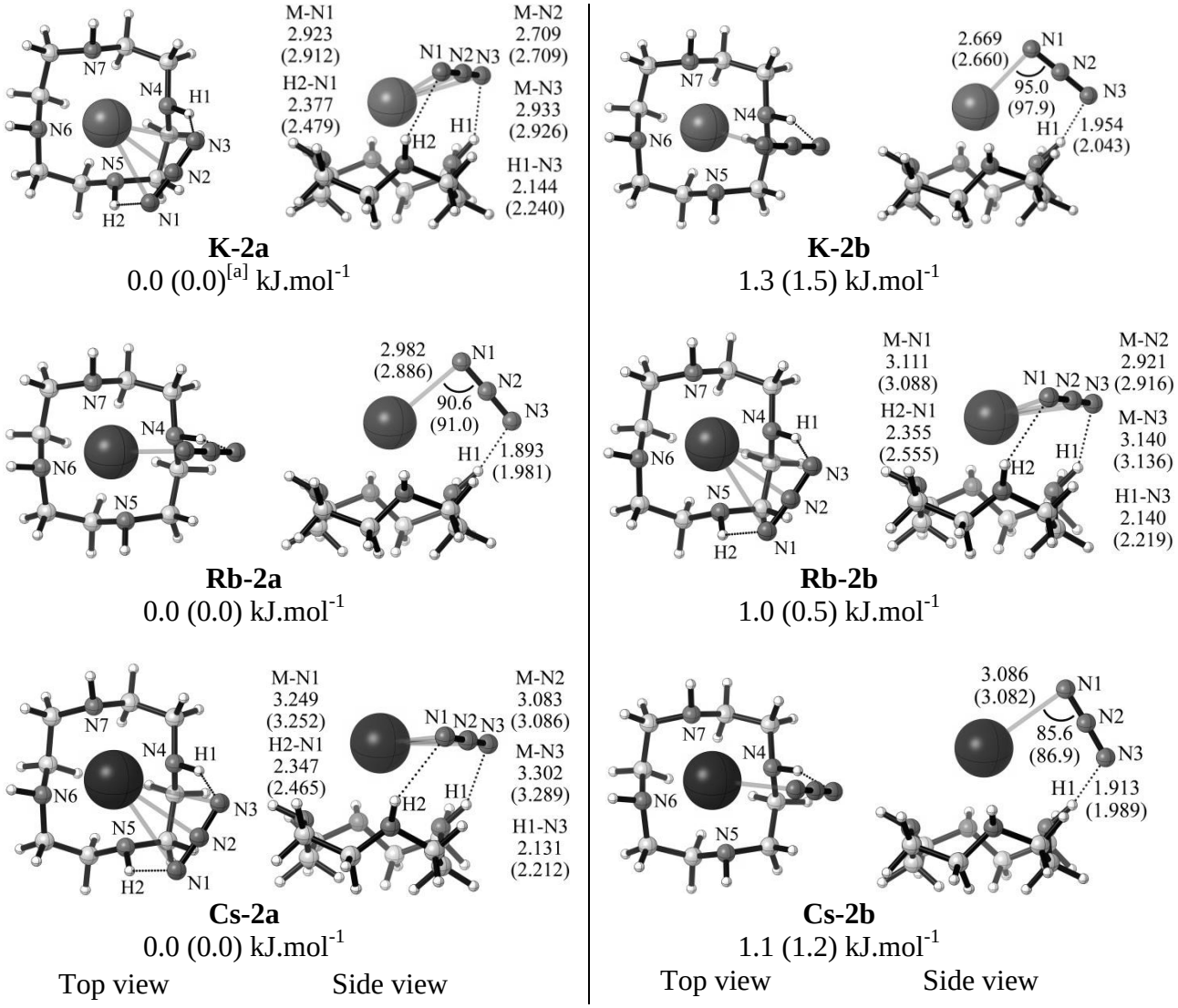

Figure 5 Optimised geometries [BP86/6-311G(d,p)] of the competitive N_3-side-on structures (M = K, Rb, Cs). Selected BP86 and B3LYP (in bracket) bond angles (°) and bond distances (Å) are

provided. [a] The BP86 and B3LYP (in bracket) relative energies ($kJ.mol^{-1}$) indicate that the structures **M-2a** are more stable than their corresponding **M-2b** analogues.

The M^+ ions in the structures **K-2b**, **Rb-2a** and **Cs-2b** adopt a similar penta-coordinated geometry to that observed in **Li-2a** and **Na-2a**. Besides the increase in the M-N_{azide} and M-N_{cyclen} bond distances (Tables S3-S4) which is accompanied with the increasing size of the radii of the M^+ ions, minor structural differences arise on going from $Li^+ \rightarrow Cs^+$ in the N_3-side-on structures. For instance, a stepwise decrease of *ca.* 5° in the M-N1-N2 bond angle is observed from **Li-2a** → **Na-2a** and from **K-2b** → **Rb-2a** → **Cs-2b** (Tables S3-S4). A small yet consistent decrease in the H1···N3 hydrogen bond distance is also observed on going from **Li-2a** → **Na-2a** → **K-2b** → **Rb-2a** (Tables S3-S4).

Unlike in the N_3-side-on structures **K-2b**, **Rb-2a** and **Cs-2b**, the M^+ ions in **K-2a**, **Rb-2b** and **Cs-2a** are hepta-coordinated, to the four N-donor atoms of the cyclen ring and to the three N atoms of the N_3 group. The N_3 unit forms a μ-1,3-bridge between two hydrogen atoms of adjacent N-H groups in the cyclen ring (N4-H1 and N5-H2) giving rise to two hydrogen bonding interactions (H1···N3 and H2···N1). As shown in Figure 5, the H1···N3 bond distance is shorter than H2···N1 for the structures **K-2a**, **Rb-2b** and **Cs-2a**. This indicates that the strengths of the two hydrogen bonding interactions are not the same. The M-N1-N2-N3 fragment of **K-2a**, **Rb-2b** and **Cs-2a** adopts a triangular side-on conformation comparable to those previously reported for the corresponding molecular alkali metal azides.[31] Reasonable points of similarity with known N_3 structures can be highlighted in terms of structural parameters. For example, the N-N-N bond angle in the molecular KN_3, RbN_3 and CsN_3 species was reported[31] to be in the range of 169–175°, while those of structures **K-2a**, **Rb-2b** and **Cs-2a** are *ca.* 176° (Tables S3-S4). Further, the N-Cs-N bond angle in CsN_3 (45.3°)[31] is slightly larger than the N1-Cs-N3 bond angle in **Cs-2a** (BP86, 42.8°; B3LYP, 42.4°).

The cavity/ion-radius ratio is likely to be the main factor in determining the lowest minimum energy structure and in this context, a direct relationship between the ionic radii of M^+ ions, M-N_{donor} bond distances and cavity sizes has been reported [32] Indeed, the mean cavity size of the cyclen ring of the N_3-side-on structures expands with an increase in the ionic size of the M^+ ions, thus showing the flexibility of the cyclen ring (Table S6).

Table 2 The distance (Å) between the plane of the four N-donor atoms of the cyclen ring and the M^+ ions of the lowest minimum energy N_3-side-on structures.

N_3-side-on structures	**Li-2a**	**Na-2a**	**K-2a** (**K-2b**)[a]	**Rb-2a** (**Rb-2b**)	**Cs-2a** (**Cs-2b**)
BP86/6-311G(d,p)	0.884	1.338	1.879 (1.889)	2.158 (2.140)	2.399 (2.430)
B3LYP/6-311G(d,p)	0.874	1.322	1.896 (1.903)	2.172 (2.157)	2.436 (2.457)

[a] The distance (Å) corresponding to the competitive N_3-side-on structures is reported in brackets.

The $M\text{-}N_{azide}$ bond distance is considerably shorter than the corresponding $M\text{-}N_{cyclen}$ bond distances in the N_3-side-on structures **Li-2a**, **Na-2a**, **K-2b**, **Rb-2a** and **Cs-2b**. This reflects strong interaction between the M^+ ions and the N1 atom of the N_3 unit. In contrast, the $M\text{-}N_{azide}$ and $M\text{-}N_{cyclen}$ bond distances in **K-2a**, **Rb-2b** and **Cs-2a** are comparable. The same trend (as in the **K-2a**, **Rb-2b** and **Cs-2a**) can be observed in the corresponding alkali metal azide-crown ether complexes.[4a]

(d) Comparison between the lowest minimum energy structures of N_3-end-on and N_3-side-on [M(cyclen)N_3], M = Li-Cs

The energies of the lowest minimum energy N_3-end-on structures relative to their N_3-side-on analogues are compared in Table 3. For all the [M(cyclen)N_3] complexes (M = Li-Cs), the N_3-side-on structure is energetically lower than the N_3-end-on structure.

Table 3 The relative energies ($kJ.mol^{-1}$) of the lowest minimum energy N_3-end-on and N_3-side-on structures obtained using the BP86/6-311G(d,p) method; the N_3-side-on structure is lower than the N_3-end-on structure in all cases.

N_3-end-on structures	N_3-side-on structures	Relative energy[a] ($kJ.mol^{-1}$)
Li-1a	**Li-2a**	9.1 (4.9)
Na-1a	**Na-2a**	13.6 (11.2)
K-1a	**K-2a**	11.1 (9.5)
Rb-1a	**Rb-2a**	12.3 (10.6)
Cs-1a	**Cs-2a**	10.5 (10.2)

[a] The B3LYP relative energies ($kJ.mol^{-1}$) are given in brackets.

The cyclen unit of both the N_3-end-on and N_3-side-on structures adopts a C_4(++++) conformation, as has recently been reported for crystal structures[8g,12] of three functionalised

alkali metal-cyclen complexes. These are the $[Li(Me_4cyclen)(OH_2)][BAr^F]$,[12] $[Na(Me_4cyclen)(thf)][BAr^F]$[12] and $[Na(Me_3cyclen)I]$[8g] complexes, where Me_4cyclen = 1,4,7,10-tetramethyl-1,4,7,10-tetraazacyclododecane and Me_3cyclen = 1,4,7-trimethyl-1,4,7,10-tetraazacyclododecane. The Li-N_{cyclen}/Na-N_{cyclen} bond distances of these three crystal structures agree well with the corresponding bond distances of the N_3-side-on structures **Li-2a** and **Na-2a** (Tables S3-S4). However, the distance between the basal plane of the cyclen ring and Li^+/Na^+ ion is slightly larger in **Li-2a** and **Na-2a** (Table 2), when compared with these distances in the three functionalised alkali metal-cyclen complexes [0.758(7),[12] 1.225(2)[12] and 1.2803(11)[8g] Å, respectively].

The N_3-side-on structures **M-2a** (M = Li, Na, Rb) and **M-2b** (M = K, Cs) are similar to some crystal structures of transition metal azide-NNNN containing macrocycles.[11a-f,h,j] The N_3 unit of these structures adopts a side-on conformation similar to that in the transition metal tetraaza analogues. However, the M-N-N bond angle is larger in these transition metal azides with M-N-N bond angles ranging from 121.3(2)° to 149.7(8)° for M = Co, Fe, Cu, Cr, Mn and Ru,[11a-f,h,j] compared to 101.6–85.6° (BP86; B3LYP, 104.2–86.9°) for the alkali metal N_3-side-on structures investigated in this work (Tables S3-S4). Several transition metal azide crystal structures[11a-e] have the cyclam unit (1,4,8,11-tetraazacyclotetradecane) as the macrocycle, which has four N-H groups as potential coordinating groups. However, no hydrogen bond interaction has been observed between the N-H and N_3 groups in these compounds.[11a-e]

(e) Sandwich $[M(cyclen)_2N_3]$ structures, M = Li-Cs

Optimisation calculations were also performed on sandwich structures of the type $[M(cyclen)_2N_3]$, where N_3 is trapped between two cyclen units, to see if structures can be located which bind N_3 and give rise to loss of nitrogen *via* low energy pathways (*e.g. via* dissociations of the type given in equations 2 and 3). Two sandwich structures, denoted as **M-3a** and **M-3b** (M = Li-Cs), were found to be minimum energy structures. The BP86 optimised geometries of **M-3a** and **M-3b** are depicted in Figures 6 and S15, respectively. For each alkali metal, structure **M-3a** is lower in energy than **M-3b** (Table S7) and hence, only the **M-3a** structures will be discussed in this work.

Li-3a

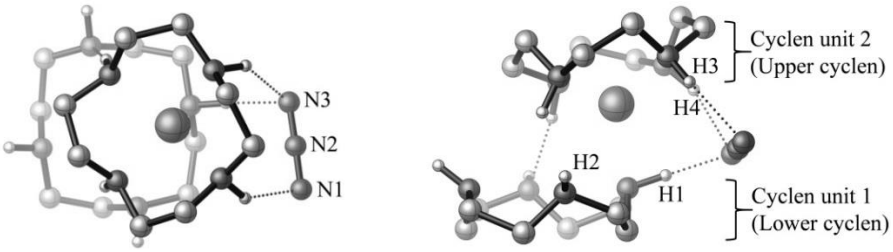

Na-3a

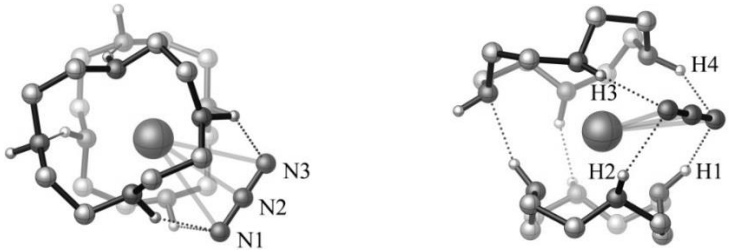

K-3a

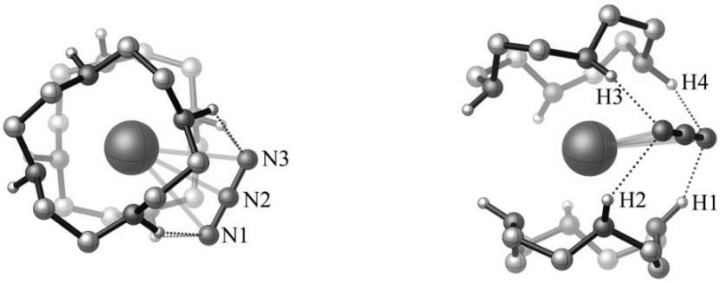

Rb-3a

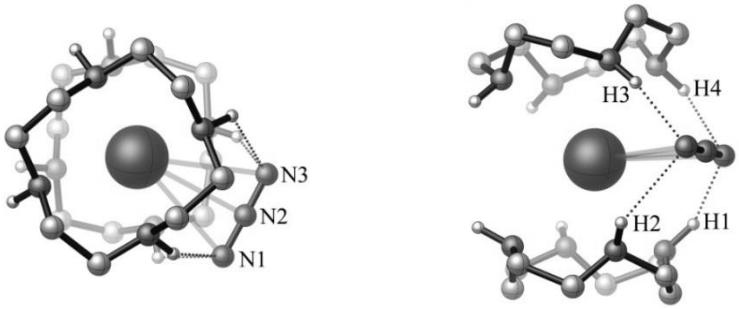

Cs-3a

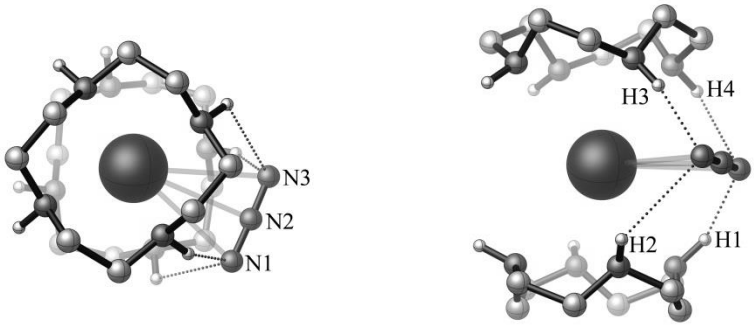

Top view Side view

Figure 6 Optimised geometries [BP86/6-311G(d,p)] of the sandwich structures. Selected hydrogen atoms are omitted for clarity.

The structure **Li-3a** is distinctive among the sandwich [M(cyclen)$_2$N$_3$] complexes. The small Li^+ ion does not allow the lower and upper cyclen units to align above each other. One of the cyclen units is displaced such that all four N-donor atoms of the upper cyclen unit interact fully with the Li^+ ion, while the lower cyclen unit interacts only partially with Li^+. The sandwich structures **M-3a**, for M = Na-Cs, are isostructural. They have C_2 symmetry. As expected with an increase in the size of the ionic radii of the M^+ ions, the M-N_{cyclen} bond distances increase on going from **Na-3a** to **Cs-3a** (Table S8). This is subsequently accompanied by an increase in the acuteness of the N-M-N bond angle of the five-membered ring, which is defined by the N-C-C-N moiety of the cyclen ring and the M^+ ion (Table S8). Thus, going down the **M-3a** series, the lower and upper cyclen units become more separated from each other and this allows the interaction between the M^+ ions and N_3 unit to increase. The two cyclen units in the structures **Li-3a** and **Na-3a** are close enough to allow hydrogen bonding interactions between their respective N-H moieties. The M-N_{azide} bond distances decrease from **Li-3a** → **Na-3a** → **K-3a** and then increase to **Rb-3a** and **Cs-3a**, respectively (Tables 4 and S8). Further, the Li-N_{azide} bond distances of the structure **Li-3a** are longer than the sum of the van der Waal's radii of Li and N.[33] This suggests the presence of very weak interaction between the Li^+ ion and the N_3 unit. The structure **Li-3a** has only three hydrogen bonding interactions between the cyclen units and the N_3 unit, while the structures **M-3a**, for M = Na-Cs, have four such interactions and their distances range from 1.842 to 2.902 Å (BP86; B3LYP, 1.900 to 2.966 Å). In general, the M-N_{azide} bond distances of the structures **M-3a**, for M = Na-Cs, are longer than their corresponding M-N_{cyclen} bond distances (except for M-N7 and M-N10, see Figure S15 for atom labeling and Tables 4 and S8). This shows that addition of a second cyclen unit to yield the sandwich structures causes the bond strength between the M^+ ions (M^+ = Li^+-Cs^+) and the N_3 unit to weaken.

Table 4 Selected BP86 bond distances (Å) of the lowest minimum energy sandwich structures.

	Li-3a	**Na-3a**	**K-3a**	**Rb-3a**	**Cs-3a**
M-N1[a]	3.917 (3.967)	3.340 (3.385)	3.286 (3.269)	3.377 (3.331)	3.483 (3.475)
M-N2	3.454 (3.510)	3.123 (3.179)	3.070 (3.060)	3.171 (3.131)	3.289 (3.288)
M-N3	3.348 (3.388)	3.340 (3.385)	3.286 (3.269)	3.377 (3.331)	3.483 (3.475)
H1-N3	1.842 (1.900)	2.178 (2.233)	2.079 (2.147)	2.099 (2.191)	2.080 (2.151)

H2-N1	4.822 (4.828)[b]	2.232 (2.291)	2.413 (2.494)	2.581 (2.653)	2.902 (2.966)
H3-N1	2.086 (2.137)	2.178 (2.233)	2.079 (2.147)	2.099 (2.191)	2.080 (2.151)
H4-N3	2.216 (2.293)	2.232 (2.291)	2.413 (2.494)	2.581 (2.653)	2.902 (2.966)

[a] The bond distances (Å) obtained using the B3LYP functional are reported in brackets.
[b] The H2-N1 bond distance does not correspond to hydrogen bonding in structure **Li-3a**.

3.2 Bonding Analysis

A reasonable description of the electronic structures of the N_3-end-on, N_3-side-on and sandwich complexes can be obtained from natural population analysis (NPA) within the NBO framework. The NPA charges on all the centres of the optimised (a) 'free' cyclen ligand, (b) M^+(cyclen) structures, (c) N_3-end-on structures, (d) N_3-side-on structures and (e) sandwich structures (M^+ = Li^+-Cs^+) are gathered in SI (BP86 results, Tables S10-13; B3LYP results, Tables S15-S18).

Electron density transfer from the ligands (cyclen and/or azide) to the M^+ ions in the M^+(cyclen), N_3-end-on, N_3-side-on and sandwich structures (M^+ = Li^+-Cs^+), is clearly indicated upon analysis of the NPA charges. This transfer can be quantified by the difference between the initial formal charge on the alkali metal cations (+1) and the NPA charge on the metal in the corresponding complex. Electron density is mainly transferred from firstly, the σ C-N and σ N-H bonding orbitals and the N 2p non-bonding orbitals of the cyclen ring and/or secondly, from the N 2p non-bonding orbitals of the N_3 ligand to the available orbitals of the M^+ ions in the M^+(cyclen), N_3-end-on, N_3-side-on and sandwich structures for M^+ = Li^+-Cs^+ (Tables S20-S23 for active orbitals of M^+). The N_3 unit in the end-on, side-on and sandwich structures is characterised by alternating net charges $N1^{(\delta-)}$-$N2^{(\delta+)}$-$N3^{(\delta-)}$ along the N_3 unit. The electron poor M^+ ion and the hydrogen bond donor fragment (N4-H1) withdraw electron density from the adjacent N atom (N1) of the N_3 unit in the end-on structures (Figures 2b and 3). The electron cloud of the N_3 unit tends to concentrate on its N1 atom and as a result N1 is more negatively charged than the terminal N3 atom. The NPA charges on the N1 atoms of the N_3-end-on structures increase on going from **Li-1a**/**Li-1b** → **Na-1a** → **K-1a** → **Rb-1a** → **Cs-1a** (Tables S11 and S16), correlating with less electron density being transferred from the N1 2p non-bonding orbitals to the available orbitals of M^+ as the ionic radii of the M^+ ions increase. The NPA charges on N1 and N3 of the terminal N atoms are clearly different for the N_3-end-on structures. In contrast, a relatively small difference is observed between the NPA charges of the

N1 and N3 atoms in the N_3-side-on structures (Tables S12 and S17). Unlike in the N_3-end-on structures, the N_3 unit in the side-on structures adopts a bridging conformation such that both terminal N atoms (N1 and N3) contribute to the transfer of electron density to the M^+ and cyclen units. In fact, the NPA charges of the terminal N atoms (N1 and N3) of the sandwich structures are the same, as expected, given that the **M-3a** structures for M = Na-Cs are centrosymmetric about their M^+ centres (Tables S13 and S18). Upon complexation, the M^+ ions in the sandwich structures **M-3a** are less positively charged than the M^+ ions in the N_3-side-on structures and this shows that more electron density is being accepted by the M^+ ions in the sandwich structures. Also, the N atoms of the cyclen units of the sandwich structures are less negatively charged than that of the N_3-side-on structures, further indicating that more electron density is being transferred to the M^+ ions in the sandwich structures **M-3a**. This indicates that the addition of a second cyclen unit adds some extra stability to the $[M(cyclen)_2]^+$ backbone of the sandwich structures **M-3a**.

3.3 Computed IR Spectra

Computed IR spectra for the N_3-end-on, N_3-side-on and sandwich structures are shown in Figure 7, obtained using the BP86/6-311G(d,p) method. The corresponding IR spectra obtained using the B3LYP/6-311G(d,p) method are displayed in Figure S16. These spectra should be useful to distinguish between the N_3-end-on, N_3-side-on and sandwich structures prepared for a given metal.

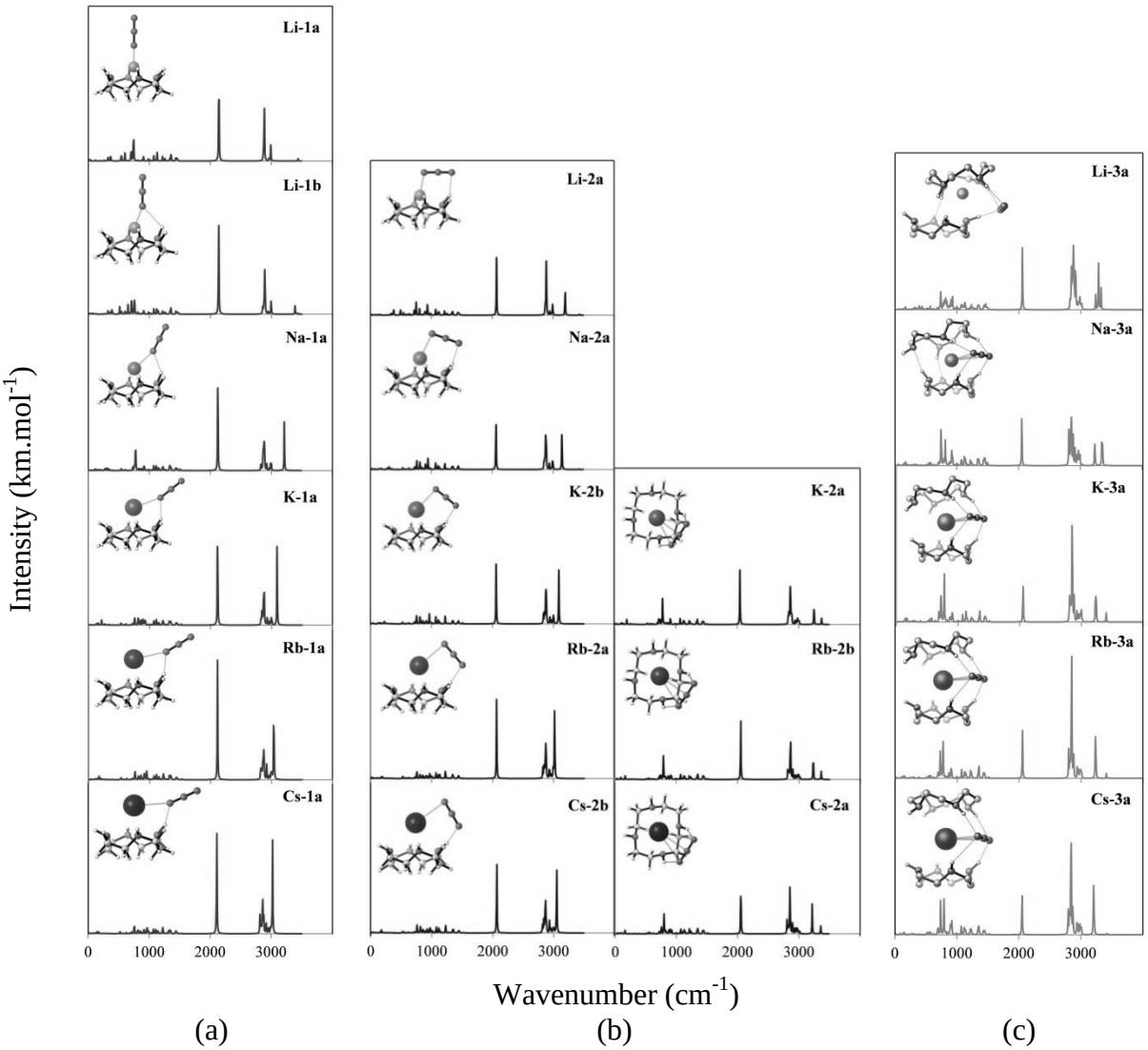

Figure 7 Comparison of IR spectra of (a) N_3-end-on and (b) N_3-side-on [M(cyclen)N_3] and (c) sandwich [M(cyclen)$_2N_3$] structures for M = Li-Cs, obtained using the BP86/6-311G(d,p) method.

These spectra consist of distinct regions, notably 2000–2200 cm^{-1} which contains a sharp intense N_3 asymmetric stretching absorption, 2800–3100 cm^{-1} which contains a number of C-H stretching absorptions, 2900–3300 cm^{-1} which contains a number of N-H absorptions and 300–1200 cm^{-1} which is the fingerprint region. Although the detailed computed positions and intensities will be essential to distinguish different structural types, a number of general features can be identified in the computed spectra. For the N_3-end-on structures, the asymmetric N_3 feature is the most intense absorption. For the N_3-side-on and sandwich structures, the N_3 asymmetric stretch is comparable in intensity to the intensity of the C-H and N-H absorptions

with the C-H absorptions being much stronger in the sandwich structures than the N-H absorptions.

For example for the sandwich structures, computed IR spectra of **Li-3a** and **Na-3a** consist of several N-H stretching absorptions, some of which overlap each other as shown in Figures 7 and S16. The N-H stretching features pertaining to hydrogen bonding between the N-H moieties of the lower and upper cyclen rings in **Li-3a** and **Na-3a** (Figure 6) are at a higher energy compared to those between the N-H of the cyclen rings and the N atoms of the N_3 unit. Unlike **Li-3a**, the sandwich structures **M-3a** (M = Na-Cs) adopt C_2 symmetry. Owing to their symmetry, the IR spectra of the structures **M-3a** (M = Na-Cs) consist of unique symmetric and asymmetric *trans* N-H stretching modes (N4-H1/N9-H3 and N5-H2/N8-H4). The *trans* N4-H1/N9-H3 stretching features are found at a lower energy, and they are more intense, compared to those of N5-H2/N8-H4. This indicates that the hydrogen bonds associated with the N4-H1 and N9-H3 functional groups are much stronger than the ones associated with N5-H2 and N8-H4, again consistent with the corresponding hydrogen bond distances (Table S25).

More details on the assignments of these spectra are given in SI and Tables S25-S26.

3.4 Trends in the BDEs

The N_3 unit in the end-on, side-on and sandwich structures can be envisaged as a prospective source for the formation of polymeric nitrogen. The dissociation of these structures can either lead to the formation of the N_3 radical or the dinitrogen molecule from N-N_2 cleavage. In this work, the BDEs for the processes (1), (2) and (3) were calculated using the BP86/6-311G(d,p) and B3LYP/6-311G(d,p) methods, with more reliable values for process (1) computed at the DF-L(U)CCSD(T) level as a check on the DFT values. Table 5 [process (1)] shows the calculated BP86, B3LYP and DF-L(U)CCSD(T) BDEs for the N_3-end-on and N_3-side-on structures. The calculated BDEs obtained at different levels are consistent, with the DF-L(U)CCSD(T) BDE values always being slightly higher than the BP86 and B3LYP values. Table 5 shows computed BDEs obtained with the DF-L(U)CCSD(T) method with ACVDZ and ACVTZ basis sets. In each case, these values were used to obtain the extrapolated CBS value using the method described in the Computational Detail. These CBS values show the BP86 and B3LYP values to be reliable, but slightly low. The BDEs are consistent with the fact that the N_3-side-on structures **M-2a** (M = Li-Cs) and **M-2b** (M = K-Cs) are more stable than their

corresponding N_3-end-on structures **M-1a** (M = Li-Cs) and **Li-1b**. Consistent with the literature,[14a] a relationship between the BDE values and the distances between the alkali metal and the terminal N atoms (M-N1), for the N_3-end-on and N_3-side-on [M(cyclen)N_3] structures (M = Li-Cs), are observed along the alkali metal series. In general, the BDE values, associated with process (1), decrease with a systematic lengthening of the M-N1 bond necessitated by an increase in the size of the ionic radii of the M^+ ions (0.60, 0.98, 1.33, 1.49 and 1.69 Å,[9a,34] respectively) on going from $Li^+ \rightarrow Cs^+$.

Table 5 The calculated bond dissociation energies (kJ.mol^{-1}) of the lowest minimum energy N_3-end-on and N_3-side-on structures for the process $[M(cyclen)(N_3)]_{(g)} \rightarrow M(cyclen)_{(g)} + N_{3(g)}$ (1).

	N_3-end-on structures				
	Li-1a(Li-1b)[a]	**Na-1a**	**K-1a**	**Rb-1a**	**Cs-1a**
BP86	384.1 (383.0)	353.7	345.4	322.5	321.2
B3LYP	389.5 (–)	351.8	335.6	312.3	308.9
DF-L(U)CCSD(T)					
(a) ACVDZ	401.2 (399.2)	363.1	352.9	359.6	352.6
(b) ACVTZ	406.4 (409.6)	377.2	368.9	365.6	369.0
(c) CBS	408.6 (414.0)	383.1	375.6	368.2	375.9
	N_3-side-on structures				
	Li-2a	**Na-2a**	**K-2a** (**K-2b**)	**Rb-2a** (**Rb-2b**)	**Cs-2a** (**Cs-2b**)
BP86	393.2	367.3	356.5 (355.2)	334.8 (333.8)	331.7 (330.8)
B3LYP	394.4	362.9	345.1 (343.7)	322.9 (322.5)	319.1 (317.9)
DF-L(U)CCSD(T)					
(a) ACVDZ	408.3	376.0	373.4 (364.1)	362.1 (375.7)	374.0 (361.6)
(b) ACVTZ	422.9	389.4	390.7 (383.7)	375.5 (391.4)	395.5 (377.3)
(c) CBS	429.0	395.0	398.0 (391.9)	381.2 (397.9)	404.5 (384.0)

[a] The BDE values (kJ.mol^{-1}) corresponding to the competitive N_3-end-on and N_3-side-on structures are reported in brackets.

The release of dinitrogen molecule from the N_3-end-on and N_3-side-on structures, represented by process (2) (Table 6), is significantly less endothermic than process (1). The BDE values in Table 6 for process (2) again highlight the higher stability of the N_3-side-on structures over their N_3-end-on form. The dissociation energies for process (3), the release of the N_3 molecule from the parent sandwich structures **M-3a** (M = Li-Cs), are shown in Table 7. No particular trend in the BDE values can be discerned from these values.

Table 6 The calculated bond dissociation energies (kJ.mol^{-1}) of the lowest minimum energy N_3-end-on and N_3-side-on structures for the process $[M(cyclen)(N_3)]_{(g)} \rightarrow M(cyclen)N_{(g)} + N_{2(g)}$ (2).

	N_3-end-on structures				
	Li-1a(Li-1b)	**Na-1a**	**K-1a**	**Rb-1a**	**Cs-1a**
BP86	64.3 (63.2)[a]	70.2	58.1	68.9	68.5
B3LYP	42.9	47.0	34.2	44.6	43.8
	N_3-side-on structures				
	Li-2a	**Na-2a**	**K-2a** (**K-2b**)	**Rb-2a** (**Rb-2b**)	**Cs-2a** (**Cs-2b**)
BP86	73.4	83.8	69.2 (68.0)	81.2 (80.2)	79.0 (78.0)
B3LYP	47.9	58.2	43.8 (42.3)	55.2 (54.8)	54.0 (52.8)

[a] The BDE values (kJ.mol^{-1}) corresponding to the competitive N_3-end-on and N_3-side-on structures are reported in brackets.

Table 7 The calculated bond dissociation energies (kJ.mol^{-1}) of the lowest minimum energy sandwich structures for the process $[M(cyclen)_2(N_3)]_{(g)} \rightarrow M(cyclen)_{2(g)} + N_{3(g)}$ (3).

	Li-3a	**Na-3a**	**K-3a**	**Rb-3a**	**Cs-3a**
BP86	161.1	155.3	151.7	157.3	147.6
B3LYP	176.0	163.1	164.4	173.8	157.2

These results indicate that loss of N_3 from the sandwich structures is more favourable energetically (less endothermic) than loss of N_3 from the N_3-end-on and N_3-side-on structures. Loss of N_2 from the N_3-end-on and N_3-side-on structures is also much less endothermic than loss of N_3 from these structures. This is also expected to be the case for the sandwich structures although no calculations have been carried out on N_2 loss in these cases.

Table 8 Comparison of BP86 M-$N_{terminal\ azide}$ computed bond distances and computed natural metal-nitrogen charge densities for MN_3, N_3-end-on and N_3-side-on $[M(cyclen)N_3]$ compounds, and the sandwich $[M(cyclen)_2N_3]$ compounds.

Compound	M-N1 distance (Å)	Charge (e) on			Comments
		M	N1	N3	
LiN_3	1.715	0.859	-0.821	-0.240	Linear
NaN_3	2.065	0.908	-0.797	-0.296	Linear
KN_3	2.347	0.935	-0.800	-0.317	Linear
RbN_3	2.942	0.975	-0.529	-0.529	Triangular
CsN_3	3.087	0.980	-0.533	-0.533	Triangular

N_3-end-on [M(cyclen)N_3] structures					
Li-1a	1.864	0.472	-0.593	-0.339	
Na-1a	2.251	0.677	-0.667	-0.329	
K-1a	2.570	0.802	-0.696	-0.333	
Rb-1a	2.770	0.926	-0.712	-0.347	
Cs-1a	2.927	0.942	-0.711	-0.352	
N_3-side-on [M(cyclen)N_3] structures					
Li-2a	2.005	0.524	-0.504	-0.430	
Na-2a	2.340	0.681	-0.512	-0.459	
K-2a	2.923	0.772	-0.475	-0.490	
Rb-2a	2.892	0.923	-0.524	-0.505	
Cs-2a	3.249	0.944	-0.507	-0.526	
Sandwich [M(cyclen)$_2$$N_3$] structures					
Li-3a	3.917	0.468	-0.440	-0.523	
Na-3a	3.340	0.459	-0.475	-0.475	
K-3a	3.286	0.539	-0.479	-0.479	
Rb-3a	3.377	0.865	-0.507	-0.507	
Cs-3a	3.483	0.888	-0.507	-0.507	

The agreement between the structural parameters and relative energies obtained from calculations with the two functionals (BP86, a GGA functional, and B3LYP, a hybrid functional) is summarised in Figures 1-5 and Tables 1-7, and in the SI. The agreement between the sets of computed values obtained with the two functionals is good. In general, the B3LYP dissociation energies are slightly lower than the BP86 values for dissociations (1) and (2), and slightly higher than the BP86 values for dissociation (3). Also, for the N_3-end-on and N_3-side-on [M(cyclen)N_3] structures for M = Li-Cs, as shown in Table 3, the B3LYP relative energies are slightly lower than the BP86 relative energies, with the N_3-side-on structure being lower in each case.

4.0 Conclusions

Table 8 shows for M = Li-Cs, the computed M-$N_{terminal}$ distances for the isolated azides MN_3, and for the lowest energy minimum energy structures of end-on [M(cyclen)N_3], side-on [M(cyclen)N_3], and the sandwich [M(cyclen)$_2$$N_3$] compounds, as well as the computed natural charges for the terminal N atoms of the azide group (N1 and N3) in these compounds. The effect of the cyclen $\rightarrow$ M electron transfer in reducing the natural charges on the metal in the cyclen complexes compared to those in the parent azide MN_3 is clearly evident. For Li, Na and K, the

M-N1 bond distances are in the order MN_3 < end-on [M(cyclen)N_3] < side-on [M(cyclen)N_3] < [M(cyclen)$_2N_3$] sandwich. However, for Rb and Cs, the M-N1 bond lengths are similar for MN_3, end-on [M(cyclen)N_3] and side-on [M(cyclen)N_3] with the sandwich [M(cyclen)$_2N_3$] values being clearly larger. The reduced differences in the M-N1 distances between the MN_3 azides and the end-on and side-on [M(cyclen)N_3] compounds for Rb and Cs compared to Li, Na and K, is probably attributable to the decreased charge/radius ratio in Rb and Cs, which makes these alkali metals less sensitive to their surrounding ligands than Li, Na and K. Inspection of Table 8 also shows that the sandwich [M(cyclen)$_2N_3$] structures have a different charge distribution from the end-on and side-on [M(cyclen)N_3] structures. Addition of a second cyclen unit to [M(cyclen)N_3] gives rise to extra electron transfer to the metal from the second cyclen unit, and this results in a lower positive charge on the metal and a reduced bond strength between the metal and the N_3 unit. This can be seen in Table 8 for the sandwich structures which have longer M-N1 distances, less positive metal charges and less negative charges on N1 than the [M(cyclen)N_3] structures. Major factors in determining the geometries of these compounds appear to be the metal/charge radius ratio and the size of the cyclen cavity, with hydrogen bonding making a small contribution. Of the three dissociation processes considered (1) loss of N_3 from the end-on and side-on [M(cyclen)N_3] complexes, (2) loss of N_2 from the end-on and side-on [M(cyclen)N_3] complexes, and (3) loss of N_3 from the M(cyclen)$_2N_3$ sandwich structures, the least endothermic process is (2) and the most endothermic process is (1). As expected, N_3 is lost more easily from the sandwich compounds than from the end-on and side-on [M(cyclen)N_3] complexes.

The first [M(cyclen)N_3] compound to synthesise is probably the Na complex at the reagents (NaN_3 and cyclen) are readily available and the relative energy between the N_3-side-on and N_3-end-on structures is expected to be the largest for M = Na (Table 3), with the N_3-side-on structure the lower. The method would follow that used for the [M(crown ether)N_3] complexes,[4a] *i.e.* reaction of NaN_3 with cyclen in a suitable solvent. Diethyl ether, tetrahydrofuran and methanol should all be tried but interaction of O-donor solvents such as these with the metal cation (M^+) may limit the interaction of M^+ with the cyclen ligand. Hence other solvents such as toluene and dichloromethane may be more appropriate. The choice of solvent for the MN_3 + cyclen reaction to make [M(cyclen)N_3], and the subsequent concentration of the solution to enable [M(cyclen)N_3] crystals to be obtained are expected to be the main challenges.

The main experimental methods which will be used to investigate the structures obtained will be X-ray diffraction and IR spectroscopy. Once single crystals are obtained, X-ray structures will be obtained which can be compared with the computed structures, as has been achieved for the corresponding alkali metal [M(crown ether)N_3] complexes, to gain further insight into the structure and bonding in these complexes. IR spectra will also be recorded on the crystals obtained. As already stated, this will be valuable to distinguish between the N_3-end-on, N_3-side-on and sandwich structures prepared for a given metal. It will also be valuable to probe the interaction of the N_3 unit with the cyclen N-H hydrogen atoms in these complexes. This should be of interest to biochemists and supramolecular chemists as interactions of this type should occur in other metal centred complexes of importance to these communities.

In conclusion, the answer to the question posed at the start of this paper "Can cyclen (1,4,7,10-tetraazacyclododecane) bind alkali metal azides?" is "Yes" – but the appropriate experimental conditions will have to be chosen and the experiments carried out carefully.

5.0 Acknowledgements

[†]The authors acknowledge the use of the EPSRC UK National Service for Computational Chemistry Software (NCCS).

This work was also supported by funding provided by the Tertiary Education Commission of Mauritius (TEC).

Professor William Levason (Southampton University) is thanked for valuable advice and discussions.

6.0 References

[1] (a) C. J. Pedersen, *J. Am. Chem. Soc.*, 1967, **89**, 7017; (b) G. W. Gokel, W. M. Leevy and M. E. Weber, *Chem. Rev.*, 2004, **104**, 2723.

[2] (a) G. R. C. Hamilton, S. K. Sahoo, S. Kamila, N. Singh, N. Kaur, B. W. Hylanda and J. F. Callan, *Chem. Soc. Rev.*, 2015, **44**, 4415; (b) M. C.-L. Yeung and V. W.-W. Yam, *Chem. Soc. Rev.*, 2015, **44**, 4192; (c) T.-Y. Kuo, W.-H. Tseng and C.-H. Chen, *Angew. Chem. Int. Ed.*, 2015, **54**, 9213.

[3] (a) K. Kawakami, Y. Sei, K. Yamaguchi and A. Tsuda, *J. Org. Chem.*, 2011, **76**, 875; (b) P. Cui, T. P. Spaniol, L. Maron and J. Okuda, *Chem. Commun.*, 2014, **50**, 424; (c) J. Xiong, J. Zhang, Y. Sun, Z. Dai, X. Pan and J. Wu, *Inorg. Chem.*, 2015, **54**, 1737.

[4] (a) M. D. Brown, J. M. Dyke, F. Ferrante, W. Levason, J. S. Ogden and M. Webster, *Chem. Eur. J.*, 2006, **12**, 2620; (b) N. Armata, J. M. Dyke, F. Ferrante and G. La Manna, *J. Chem. Theory Comput.*, 2008, **4**, 542; (c) M. D. Brown, M. F. Davis, J. M. Dyke, F. Ferrante, W. Levason, J. S. Ogden and M. Webster, *Chem. Eur. J.*, 2008, **14**, 2615.

[5] J. Zhang, Z. Zeng, H.-Q. Lin and Y.-L. Li, *Sci. Rep.*, 2014, **4**: 4358 and references therein.
[6] M. Everett, A. Jolleys, W. Levason, D. Pugh and G. Reid, *Chem. Commun.*, 2014, **50**, 5843.
[7] (a) G. Piersanti, F. Remi, V. Fusi, M. Formica, L. Giorgi and G. Zappia, *Org. Lett.*, 2009, **11**, 417; (b) A. J. Amoroso and S. J. A. Pope, *Chem. Soc. Rev.*, 2015, **44**, 4723.
[8] For examples on the coordination of functionalised cyclen and alkali metal ions:
(a) P. Groth, *Acta Chem. Scand. A*, 1983, **37**, 283; (b) A. K. W. Stephens, R. S. Dhillon, S. E. Madbak, S. L. Whitbread and S. F. Lincoln, *Inorg. Chem.*, 1996, **35**, 2019; (c) R. Custelcean, M. Vlassa and J. E. Jackson, *Chem. Eur. J.*, 2002, **8**, 302; (d) G. Ambrosi, P. Dapporto, M. Formica, V. Fusi, L. Giorgi, A. Guerri, M. Micheloni, P. Paoli, R. Pontellini and P. Rossi, *Chem. Eur. J.*, 2003, **9**, 800; (e) H. Kubo, T. N. Player, S. Shinoda, H. Tsukube, H. Nariai and T. Takeuchi, *Anal. Chim. Acta*, 2004, **504**, 137; (f) K. Igarashi, T. Nogamia and T. Ishida, *Chem. Commun.*, 2007, 501; (g) S. Standfuss, T. P. Spaniol and J. Okuda, *Eur. J. Inorg. Chem.*, 2010, **2010**, 2987; (h) H. Ito, H. Tsukube and S. Shinoda, *Chem. Eur. J.*, 2013, **19**, 3330; (i) S. Shinoda, *Chem. Soc. Rev.*, 2013, **42**, 1825; (j) X. Zhang, J. Yin and J. Yoon, *Chem. Rev.*, 2014, **114**, 4918; (k) H. Ito and S. Shinoda, *ChemistryOpen*, 2014, **3**, 238.
[9] (a) B. M. Rode and S. V. Hannongbua, *Inorg. Chim. Acta*, 1985, **96**, 91; (b) V. W. Ruangpornvisuti, M. M. Probst and B. M. Rode, *Inorg. Chim. Acta*, 1988, **144**, 21.
[10] (a) C. A. Austin, Y. Chen and M. T. Rodgers, *Int. J. Mass Spectrom.*, 2012, **330-332**, 27; (b) C. A. Austin, Y. Chen, C. M. Kaczan, G. Berden, J. Oomens and M. T. Rodgers, *Int. J. Mass Spectrom.*, 2013, **354-355**, 346.
[11] For studies related to transition metal azide-NNNN containing macrocycles, see:
(a) K. Meyer, J. Bendix, N. Metzler-Nolte, T. Weyhermüller and K. Wieghardt, *J. Am. Chem. Soc.*, 1998, **120**, 7260; (b) K. Meyer, E. Bill, B. Mienert, T. Weyhermüller and K. Wieghardt, *J. Am. Chem. Soc.*, 1999, **121**, 4859; (c) C. A. Grapperhaus, B. Mienert, E. Bill, T. Weyhermüller and K. Wieghardt, *Inorg. Chem.*, 2000, **39**, 5306; (d) J. Cho, J. C. Kim and A. J. Lough, *Inorg. Chem. Commun.*, 2003, **6**, 284; (e) B. Woodard, R. D. Willett, S. Haddad, B. Twamley, C. J. Gomez-Garcia and E. Coronado, *Inorg. Chem.*, 2004, **43**, 1822; (f) M. P. Donzello, L. Bartolino, C. Ercolani and C. Rizzoli, *Inorg. Chem.*, 2006, **45**, 6988; (g) D. Schröder, H. Schwarz, N. Aliaga-Alcalde and F. Neese, *Eur. J. Inorg. Chem.*, 2007, **2007**, 816; (h) C.-M. Ho, H.-C. Leung, S. Wu, K.-H. Low, Z. Lin and C.-M. Che, *Eur. J. Inorg. Chem.*, 2012, **2012**, 151; (i) J. Torres-Alacan, O. Krahe, A. C. Filippou, F. Neese, D. Schwarzer and P. Vçhringer, *Chem. Eur. J.*, 2012, **18**, 3043; (j) D. Sakow, D. Baabe, B. Böker, O. Burghaus, M. Funk, C. Kleeberg, D. Menzel, C. Pietzonka and M. Bröring, *Chem. Eur. J.*, 2014, **20**, 2913.
[12] J. M. Dyke, W. Levason, M. E. Light, D. Pugh, G. Reid, H. Bhakhoa, P. Ramasami and L. Rhyman, *Dalton Trans.*, 2015, **44**, 13853.
[13] J. Kim, M. Shamsipur, S. Z. Huang, R. H. Huang and J. L. Dye, *J. Phys. Chem. A*, 1999, **103**, 5615.
[14] (a) P. W. Schultz, D. L. Ward, A. I. Popov and G. E. Leroi, *J. Phys. Chem.*, 1996, **100**, 18083; (b) T. Akutagawa, T. Hasegawa, T. Nakamura, S. Takeda, T. Inabe, K.-I. Sugiura, Y. Sakata and A. E. Underhill, *Inorg. Chem.*, 2000, **39**, 2645; (c) T. Akutagawa, T. Motokizawa, K. Matsuura, S. Nishihara, S.-I. Noro and T. Nakamura, *J. Phys. Chem. B*, 2006, **110**, 5897.
[15] For examples on sandwich complexes of metal-NNNN macrocycles, see:
(a) Z. Valicsek, G. Eller and O. Horváth, *Dalton Trans.*, 2012, **41**, 13120; (b) W. Cao, H. Wang, X. Wang, H. Kay Lee, D. K. P. Ng and J. Jiang, *Inorg. Chem.*, 2012, **51**, 9265; (c) R. Słota, G. Dyrda, M. Hofer, G. Mele, E. Bloise and R. del Sole, *Molecules*, 2012, **17**, 10738; (d) D. Qi and J. Jiang, *ChemPhysChem*, 2015, **16**, 1889.

[16] J. P. Perdew, *Phys. Rev. B*, 1986, **33**, 8822.
[17] (a) H. B. Schlegel, *J. Comput. Chem.*, 1982, **3**, 214; (b) H. B. Schlegel, *in Modern Electronic Structure Theory* ed. D. R.Yarkony, World Scientific Publishing: Singapore, 1995, 459.
[18] W. J. Hehre, L. Radom, P. v. R. Schleyer and J. Pople, *Ab Initio Molecular Orbital Theory*, Wiley: New York, 1986.
[19] T. Leininger, A. Nicklass, W. Küchle, H. Stoll, M. Dolg and A. Bergner, *Chem. Phys. Lett.*, 1996, **255**, 274.
[20] (a) A. D. Becke, *J. Chem. Phys.*, 1993, **98**, 5648; (b) C. Lee, W. Yang and R. G. Parr, *Phys. Rev. B*, 1988, **37**, 785.
[21] (a) F. Weigend and R. Ahlrichs, *Phys. Chem. Chem. Phys.*, 2005, **7**, 3297; (b) D. Rappoport and F. Furche, *J. Chem. Phys.*, 2010, **133**, 134105.
[22] (a) A. E. Reed, R. B. Weinstock and F. Weinhold, *J. Chem. Phys.*, 1985, **83**, 735; (b) A. E. Reed, L. A. Curtiss and F. Weinhold, *Chem. Rev.*, 1988, **88**, 899.
[23] Gaussian 09, Revision D.01, M. J. Frisch, G. W. Trucks, H. B. Schlegel, G. E. Scuseria, M. A. Robb, J. R. Cheeseman, G. Scalmani, V. Barone, B. Mennucci, G. A. Petersson, H. Nakatsuji, M. Caricato, X. Li, H. P. Hratchian, A. F. Izmaylov, J. Bloino, G. Zheng, J. L. Sonnenberg, M. Hada, M. Ehara, K. Toyota, R. Fukuda, J. Hasegawa, M. Ishida, T. Nakajima, Y. Honda, O. Kitao, H. Nakai, T. Vreven, J. A. Montgomery, Jr., J. E. Peralta, F. Ogliaro, M. Bearpark, J. J. Heyd, E. Brothers, K. N. Kudin, V. N. Staroverov, R. Kobayashi, J. Normand, K. Raghavachari, A. Rendell, J. C. Burant, S. S. Iyengar, J. Tomasi, M. Cossi, N. Rega, J. M. Millam, M. Klene, J. E. Knox, J. B. Cross, V. Bakken, C. Adamo, J. Jaramillo, R. Gomperts, R. E. Stratmann, O. Yazyev, A. J. Austin, R. Cammi, C. Pomelli, J. W. Ochterski, R. L. Martin, K. Morokuma, V. G. Zakrzewski, G. A. Voth, P. Salvador, J. J. Dannenberg, S. Dapprich, A. D. Daniels, Ö. Farkas, J. B. Foresman, J. V. Ortiz, J. Cioslowski and D. J. Fox, Gaussian, Inc., Wallingford CT, 2009.
[24] (a) C. Hampel and H.-J. Werner, *J. Chem. Phys.*, 1996, **104**, 6286; (b) M. Schütz and H.-J. Werner, *Chem. Phys. Lett.*, 2000, **318**, 370; (c) M. J. Schütz, *Chem. Phys.*, 2000, **113**, 9986; (d) M. Schütz and H.-J. Werner, *J. Chem. Phys.*, 2001, **114**, 661.
[25] MOLPRO, version 2012.1, a package of *ab initio* programs, H.-J. Werner, P. J. Knowles, G. Knizia, F. R. Manby, M. Schütz and others, see http://www.molpro.net.
[26] (a) H.-J. Werner, F. R. Manby and P. J. Knowles, *J. Chem. Phys.*, 2003, **118**, 8149; (b) M. Kállay, *J. Chem. Phys.*, 2014, **141**, 244113.
[27] T. van Mourik, *J. Chem. Theory Comput.*, 2008, **4**, 1610.
[28] A. Halkier, T. Helgaker, W. Klopper, P. Jørgensen and A. G. Császár, *Chem. Phys. Lett.*, 1999, **310**, 385.
[29] (a) R. Dooley, K. Milfeld, C. Guiang, S. Pamidighantam and G. Allen, *J. Grid Comput.*, 2006, **4**, 195; (b) N. Shen, Y. Fan and S. Pamidighantam, *J. Comput. Sci.*, 2014, **5**, 576; (c) This work used the Extreme Science and Engineering Discovery Environment (XSEDE), which is supported by National Science Foundation grant number OCI-1053575.
[30] N.-K. Kim, K.-J. Chang, D. Moon, M. S. Lah and K.-S. Jeong, *Chem. Commun.*, 2007, 3401.
[31] J. S. Ogden, J. M. Dyke, W. Levason, F. Ferrante and L. Gagliardi, *Chem. Eur. J.*, 2006, **12**, 3580.
[32] P. R. Varadwaj, A. Varadwaj, G. H. Peslherbe and H. M. Marques, *J. Phys. Chem. A*, 2011, **115**, 13180.

[33] (a) The sum of the van der Waal's radii of Li/N, Na/N, K/N, Rb/N and Cs/N are 3.37[34b] (3.78),[34c] 3.82[34b] (4.16),[34c] 4.30[34b] (4.39),[34c] 4.58[34d] (4.87)[34c] and 4.98[34d] (5.14)[34c] Å, respectively; (b) A. Bondi, *J. Phys. Chem.*, 1964, **68**, 441; (c) S. Alvarez, *Dalton Trans.*, 2013, **42**, 8617; (d) M. Mantina, A. C. Chamberlin, R. Valero, C. J. Cramer and D. G. Truhlar, *J. Phys. Chem. A*, 2009, **113**, 5806.
[34] P. B. Armentrout, B. Yang and M. T. Rogers, *J. Phys. Chem. B*, 2013, **117**, 3771.